Workshop on CFD Uncertainty Analysis
Lisbon, Portugal; 21-22 October 2004

Computation of the two-dimensional flow over a hill and past a step by a ENO-type scheme

A. Di Mascio, R. Broglia, R. Muscari

Istituto Nazionale per Studi ed Esperienze di Architettura Navale, Rome, Italy

ABSTRACT

The computations of the flow over a hill (test case C-18 of the Ercoftac database) and past a backward facing step (test case C-30) are reported. The simulations were performed for all the grids supplied for the Workshop with two turbulence models, namely the one-equation model by Spalart and Allmaras (1994) and the two-equation $k-\varepsilon$ model by Chang et al. (1995). The uncertainty was estimated by means of the least squares root approach (Eca and Hoekstra, 2002, 2003)

INTRODUCTION

The present paper reports the numerical simulations of the flow over a hill (test case C-18 of the Ercoftac database) and past a backward facing step (test case C-30) proposed for the Workshop. The numerical model used in the simulations is based on the steady RANS solver developed at the INSEAN (Di Mascio et al., 2001), where the convective fluxes in the momentum equations are evaluated by means of a second order ENO scheme, whereas diffusive fluxes are discretized by a centered scheme. Convergence acceleration is achieved by means of local time stepping, an implicit Euler scheme with approximate factorization (Beam and Warming, 1978) and an efficient multi-grid technique (Favini et al., 1996).

Two different turbulence models were applied in the simulations, i.e. the one-equation model by Spalart and Allmaras (1994) and the two-equation $k-\varepsilon$ model by Chang et al. (1995).

The simulations were performed with all the grids supplied for the Workshop; therefore, the solutions considered in the following are those computed for the grids ranging from 101×101 to 401×401 for the first test case (the flow past a hill) and for from 101×101 to 241×241 for the second one (the flow over a backward facing step).

The approach used for the assessment of the numerical uncertainty is the one described in Eca and Hoekstra (2002, 2003), based on a least squares root procedure.

The paper is organized as follows: the governing equations and the numerical algorithms are briefly recalled in the first section; results for the flow over the hill are discussed in the second section, followed by the analysis of the simulations for the flow over the step in the third section; conclusions are drawn in the last section.

MATHEMATICAL MODEL

In this section all the equations and the boundary conditions implemented in the numerical model are summarized. The Navier-Stokes equations are reported first; then the governing equations for the two turbulence models used in the following are shown. A list of the boundary conditions enforced in the calculations conclude the section.

Governing equations

The turbulent motion of an incompressible viscous fluid can be described by the Reynolds averaged Navier Stokes (RANS) equations

$$\begin{aligned} &\frac{\partial u_j}{\partial x_j} = 0 \\ &\frac{\partial u_i}{\partial t} + \frac{\partial u_j u_i}{\partial x_j} + \frac{\partial p}{\partial x_i} = \frac{\partial \tau_{ij}}{\partial x_j} \qquad i = 1,2,3. \end{aligned} \tag{1}$$

A reference length l and velocity U_∞ have been chosen to make the equations non–dimensional. In the previous equations, u_i is the i–th Cartesian component of the velocity vector, p the pressure, $\tau_{ij} = \nu_t(u_{i,j} + u_{j,i})$ the stress tensor, $\nu_t = 1/Re + \nu_\tau$ the global kinematic viscosity, $Re = U_\infty l/\nu$ the Reynolds number, ν the kinematic viscosity and ν_τ the turbulent viscosity.

Turbulence models

The Spalart–Allmaras one–equation model

In this model (Spalart and Allmaras, 1994), the eddy viscosity ν_τ is computed by means of an intermediate variable $\tilde{\nu}$ and through relation:

$$\nu_\tau = \tilde{\nu} f_{v1}(\chi); \quad \chi = \frac{\tilde{\nu}}{\nu}; \quad f_{v1}(\chi) = \frac{\chi^3}{\chi^3 + C_{v1}^3} \tag{2}$$

The variable $\tilde{\nu}$ is the solution of a partial differential equation that reads

$$\begin{aligned} \frac{D\tilde{\nu}}{Dt} &= c_{b1}\left[1 - f_{t2}\right]\tilde{S}\tilde{\nu} \\ &- \left[c_{w1} f_w - \frac{c_{b1}}{k^2} f_{t2}\right]\left[\frac{\tilde{\nu}}{d}\right]^2 \end{aligned} \tag{3}$$

$$
\begin{aligned}
&+ \quad f_{t1}\Delta U \\
&+ \quad \frac{1}{\sigma}\left[\nabla\cdot((\nu+\tilde{\nu})\nabla\tilde{\nu}) + c_{b2}(\nabla\tilde{\nu})^2\right],
\end{aligned}
$$

where $\tilde{S} = S + [\tilde{\nu}/(k^2 d^2)]f_{v2}$, S is the magnitude of the vorticity vector, d the distance from the wall, $f_{t1}, f_{t2}, f_w, f_{v2}$ are functions that depends only on χ and the distance from the wall; finally, the c-s and k are constants. The first two terms in the right hand side represent production and destruction of $\tilde{\nu}$, respectively; the third one is the so-called "trip" term, that allows to specify the laminar-turbulent transition point location (in the results shown in the next section, this term was always turned off); the last part is a dissipation term, that contains also a non conservative portion $c_{b2}(\nabla\tilde{\nu})^2$ which is responsible, together with the non-linear part of the diffusion term $\nabla\cdot(\tilde{\nu}\nabla\tilde{\nu})$, for the advection of a turbulent front into non-turbulent regions.

Chang–Hsieh–Chen two–equation model

This is a two-equation $k-\varepsilon$ model proposed by Chang et al. (1995). The eddy viscosity is given by

$$
\nu_\tau = C_\mu f_\mu \frac{k^2}{\varepsilon} \tag{4}
$$

where $C_\mu = 0.09$ and

$$
f_\mu = (1 - e^{-0.0215 R_k})^2 (1 + \frac{31.66}{R_T^{5/4}}) \tag{5}
$$

with $R_k = \sqrt{k}d/\nu$ and $R_T = k^2/(\varepsilon\nu)$.

The turbulent kinetic energy k and the dissipation rate ε are the solution of the following system of equations

$$
\begin{aligned}
\frac{Dk}{Dt} &= \nabla\cdot\left[\left(\nu + \frac{\nu_\tau}{\sigma_k}\right)\nabla k\right] + \phi_T - \varepsilon \qquad (6)\\
\frac{D\varepsilon}{Dt} &= \nabla\cdot\left[\left(\nu + \frac{\nu_\tau}{\sigma_\varepsilon}\right)\nabla\varepsilon\right] \\
&+ \quad C_1 f_1 \phi_T \frac{\varepsilon}{k} - C_2 f_2 \frac{\varepsilon^2}{k} \qquad (7)
\end{aligned}
$$

where $\sigma_k = 1$, $\sigma_\varepsilon = 1.3$, $C_1 = 1.44$, $C_2 = 1.92$ and ϕ_T is

$$
\phi_T = \nu_\tau \left(u_{i,j} + u_{j,i}\right) u_{i,j}
$$

whereas the functions f_1 and f_2 are given by

$$
\begin{aligned}
f_1 &= 1 \qquad (8)\\
f_2 &= (1 - 0.01 e^{-R_T^2})(1 - 0.0631 e^{-R_k^2}) \qquad (9)
\end{aligned}
$$

Boundary conditions

The conditions enforced at the boundary are:

- *Solid wall*: velocity, turbulent kinetic energy and turbulent viscosity are set to zero, together with the normal derivative of ε
- *Inflow*: velocity, turbulent kinetic energy and turbulent viscosity are set to the prescribed values, whereas the normal derivative of the dissipation rate is set to zero; pressure is extrapolated from inner values.
- *Outflow*: velocity, turbulent kinetic energy, dissipation rate and turbulent viscosity are extrapolated from inner values, whereas pressure is set to zero.

NUMERICAL MODEL

Spatial discretization

For the numerical solution of the equations (1), the fluid domain D is partitioned into N_l structured blocks D^l, each subdivided into $N_i \times N_j \times N_k$ disjoint hexahedrons D^l_{ijk} such that $\cup D^l_{ijk} = D^l$. Conservation laws are then applied to each finite volume:

$$
\begin{aligned}
&\sum_{s=1}^{6} \int_{\mathcal{S}_s} \mathbf{U}\cdot\mathbf{n}\ \mathrm{d}S = 0 \\
&\frac{\partial}{\partial t}\int_{\mathcal{V}_{ijk}} \mathbf{U}\ \mathrm{d}V + \sum_{s=1}^{6}\int_{\mathcal{S}_s} (\mathcal{F}_c - \mathcal{F}_d)\cdot\mathbf{n}\ \mathrm{d}S = 0
\end{aligned} \tag{10}
$$

where $\mathcal{S}_s$ is the s-th face of the finite volume D_{ijk}, whose measure is $\mathcal{V}_{ijk}$.

In order to obtain second order accuracy in space, convective and viscous fluxes in the momentum equations, as well as surface integral of the velocity in the continuity equation, are computed as:

$$
\begin{aligned}
&\int_{\mathcal{S}_s} \mathbf{U}\cdot\mathbf{n} dS = u_l n_l\big|_0\ A_s + O(\Delta^2) \\
&\int_{\mathcal{S}_s} \mathcal{F}_c\cdot\mathbf{n} dS = \mathbf{F}^c_s\big|_0\ A_s + O(\Delta^2) \\
&\int_{\mathcal{S}_s} \mathcal{F}_d\cdot\mathbf{n} dS = \mathbf{F}^d_s\big|_0\ A_s + O(\Delta^2)
\end{aligned} \tag{11}
$$

where the subscript 0 means that the quantities are computed at the face center, A_s is the measure of $\mathcal{S}_s$, Δ is the diameter of $\mathcal{S}_s$ and:

$$
\mathbf{F}^c_s = \begin{pmatrix} u_1 u_l n_l + p n_1 \\ u_2 u_l n_l + p n_2 \\ u_3 u_l n_l + p n_3 \end{pmatrix} \quad \mathbf{F}^d_s = \begin{pmatrix} \tau_{1l} n_l \\ \tau_{2l} n_l \\ \tau_{3l} n_l \end{pmatrix} \tag{12}
$$

The stress tensor at the cell interface is computed as:

$$
\tau_{lm}\big|_{i+\frac{1}{2},j,k} = \nu_{i+\frac{1}{2},j,k}\left(\frac{\partial u_m}{\partial x_l} + \frac{\partial u_l}{\partial x_m}\right)_{i+\frac{1}{2},j,k} \tag{13}
$$

The derivatives of the velocity vector are obtained by means of a finite volume approximation:

$$
\left.\frac{\partial u_m}{\partial x_l}\right|_{i+\frac{1}{2},j,k} = \frac{1}{V_{i+\frac{1}{2},j,k}}\int_{\Sigma_{i+\frac{1}{2},j,k}} u_m n_l dS + O(\Delta^2) \tag{14}
$$

where the integral is extended to the volume $V_{i+\frac{1}{2},j,k}$ (whose boundary is $\Sigma_{i+\frac{1}{2},j,k}$) that includes the cell face $S_{i+\frac{1}{2},j,k}$ and is overlapped to half the cell (i,j,k) and half the cell $(i+1,j,k)$. In equation (13), $\nu_{i+\frac{1}{2},j,k}$ denotes the sum of the kinematic and turbulent viscosity at the cell face.

The computation of the convective fluxes $\mathbf{F}_s^c$ and the surface integral of the velocity in the continuity equation requires the evaluation of pressure and velocity at the face center. To this aim, a second order ENO-type scheme has been adopted (Harten et al., 1987). These schemes were originally developed for compressible fluid flows, on the basis of the hyperbolic nature of the Eulerian part of the Navier-Stokes equations. The extension to incompressible flows is possible when working in pseudo-compressible formulation.

The building block of this kind of algorithms is the Godunov scheme (1959), in which the flux vector at cell interface is computed as the solution of a Riemann problem, whose right and left states are given by the values of the numerical solution at two neighboring cell centers. For example, at the cell face $i+\frac{1}{2},j,k$:

$$\mathbf{F}^c_{i+\frac{1}{2},j,k} = \mathbf{F}^c(\mathbf{q}_l, \mathbf{q}_r) = \mathbf{F}^c(\mathbf{q}_{i,j,k}, \mathbf{q}_{i+1,j,k}) \qquad (15)$$

$\mathbf{q}$ being the vector of the state variables, which, for pseudo–compressible flows, take the form: $\mathbf{q} = (p, u_1, u_2, u_3)^T$. This scheme yields oscillation-free discrete solutions, also when the exact solutions are discontinuous. However it can be shown that the resulting scheme is only first order accurate. Higher order accurate (up to any finite order) oscillation free solutions can be obtained by modifying the evaluation of the right and left states of the Riemann problem as explained in Harten et al. (1987). In the particular case of second order accuracy, it can be shown that left and right states have to be evaluated as:

$$\begin{aligned} \mathbf{q}_l &= \mathbf{q}_{i,j,k} \quad &+\frac{1}{2}\text{minmod}(\Delta_{i-1/2}, \Delta_{i+1/2}) \\ \mathbf{q}_r &= \mathbf{q}_{i+1,j,k} \quad &-\frac{1}{2}\text{minmod}(\Delta_{i+1/2}, \Delta_{i+3/2}) \end{aligned} \qquad (16)$$

where $\Delta_{i+1/2} = \mathbf{q}_{i+1,j,k} - \mathbf{q}_{i,j,k}$ and minmod is a function that is applied to each vector component:

$$\text{minmod}(x,y) = \begin{cases} 0 & \text{if} \quad xy \le 0 \\ \text{sign}(x)\min(|x|,|y|) & \text{if} \quad xy > 0 \end{cases} \qquad (17)$$

The evaluation of the convective flux vector requires the solution of a Riemann problem at each cell interface. In order to simplify the algorithm, a second order accurate solution was used in place of the exact one, which must be computed iteratively, given the nonlinearity of the problem; details of the algorithm can be found in Di Mascio et al. (2001), where it is also proved that the scheme is formally second order accurate.

Temporal integration

Being the steady state solution the goal of the simulation, the RANS equations are rewritten in pseudo-compressible form (Chorin, 1967) in order to have an evolution equation for the pressure. The semi-discrete system of equations can be rewritten in vector form as:

$$\left.\frac{\partial \mathbf{q}}{\partial t}\right|_{ijk} + \mathcal{R}_{ijk} = \mathbf{0} \qquad (18)$$

with

$$\mathbf{q} = \frac{1}{\mathcal{V}_{ijk}} \int_{\mathcal{V}_{ijk}} (p/\beta, u, v, w)^T \, \mathrm{d}V \qquad (19)$$

and $\mathcal{R}_{ijk}$ being the flux balance on the current cell; β is the pseudo compressibility factor.

The integration with respect to time is carried out by means of an implicit Euler scheme, i.e.

$$\frac{\mathbf{q}^{m+1}_{ijk} - \mathbf{q}^m_{ijk}}{\Delta\tau} + \mathcal{R}^{m+1}_{ijk} = \mathbf{0} \qquad (20)$$

where the superscript m denotes the iteration level and $\Delta\tau$ is the (local) time step. The previous equation is then solved with respect to $\mathbf{q}^{m+1}_{ijk}$ by a scheme similar to the one proposed in Beam and Warming (1978) for compressible flows, where the equation is rewritten in "delta" form

$$\begin{aligned} &\delta\mathbf{q}^m_{ijk} + \Delta\tau \frac{\partial \mathcal{R}_{ijk}}{\partial \mathbf{q}_{rst}} (\delta\mathbf{q}^m_{rst}) = -\Delta\tau \mathcal{R}^m_{ijk} \\ &\mathbf{q}^{m+1}_{ijk} = \mathbf{q}^m_{ijk} + \delta\mathbf{q}^m_{ijk} \end{aligned} \qquad (21)$$

with $\delta\mathbf{q}^m_{ijk} = \mathbf{q}^{m+1}_{ijk} - \mathbf{q}^m_{ijk}$, and the operator on the left hand side of the previous equation is solved by an approximate factorization technique. The resulting scheme is unconditionally stable to the linear analysis. Local time step $\Delta\tau_{ijk}$ and a multi-grid technique (Brandt, 1984; Favini et al., 1996) have been used in order to improve convergence rate.

NUMERICAL RESULTS

General remarks

In what follows, the computations made with the Spalart–Allmaras model will be referred to as **SA**, whereas those in which the Chang–Hsien–Chen model was adopted with **CH**.

The numerical solutions were computed for all the grids furnished for the Workshop, by using both turbulence models. Parameters and procedures adopted are briefly summarized here.

Full Multi-grid Iteration

For all test cases, the solution was computed using a Full Approximation Storage - Full Multi-grid algorithm, i.e. for each grid

- all coarser grid levels were generated by removing every other grid point from the previous finer level;
- the solution is computed on the coarsest level first;
- for each finer sub-level, up to the finest one:
  - the first guess of the solution is obtained by interpolation from the next coarser level;
  - all coarser levels are used in a V-cycle multi-grid iteration;
  - the solution is iterated until the convergence criteria is fulfilled.

In all the computations reported, three smoothing steps were used on each sub-levels in the V-Cycle. The pseudo-compressibility factor was always set to 1, and the (local) time step was chosen to be 25 times larger than the maximum admissible time step for the corresponding explicit Euler scheme. The CPU time required on a Pentium III (1GHz) processor for the simulation with SA for the finest grids was about 1 hour for the simulation of the flow over the step and about 2 hours for the flow over the hill; it was up to three times larger with CH. No attempt was done to optimize the convergence rate.

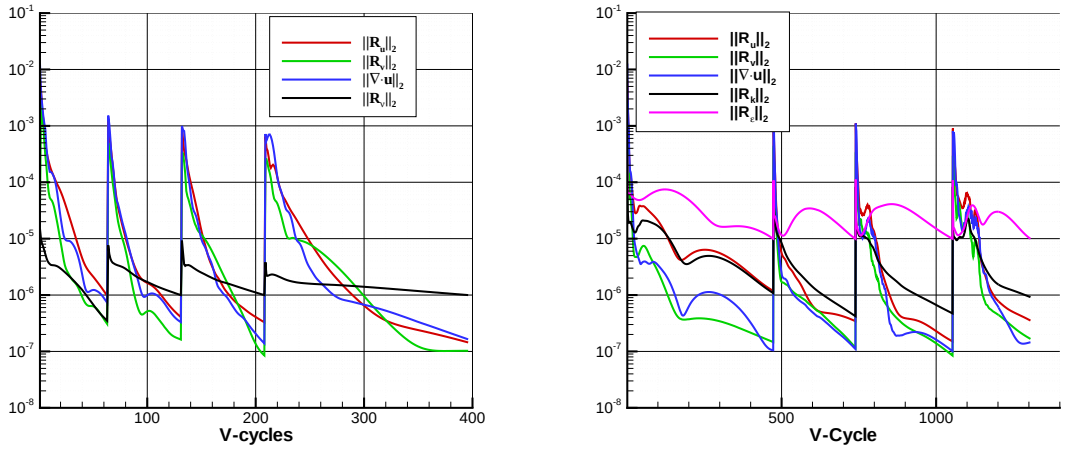

Figure 1: Step: Grid 201 × 201 ; Residual for SA (left) and CH (right)

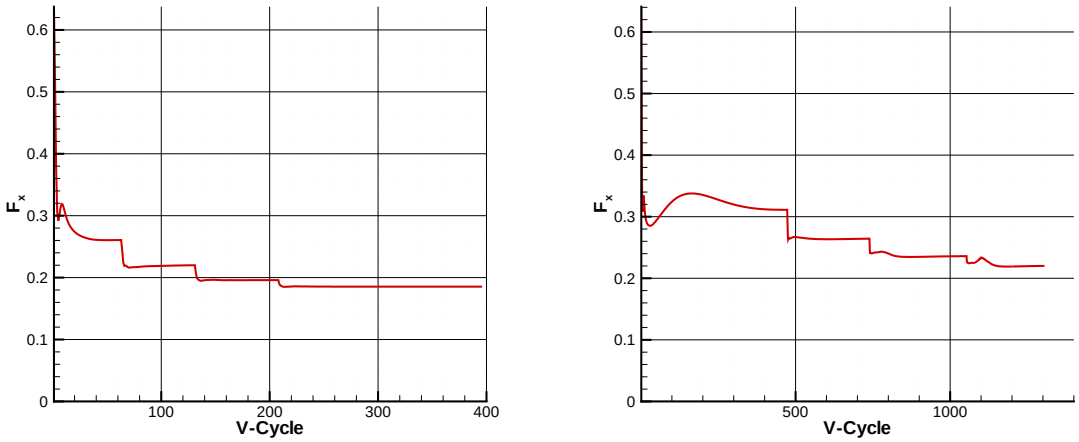

Figure 2: Step: Grid 201 × 201 ; total X force for SA (left) and CH (right)

Convergence Criteria

The iteration was stopped when all normalized residuals in L_2 norm were smaller than 10^{-6} when using the Spalart–Allmaras model (SA) and smaller than 10^{-5} with the Chang–Hsien–Chen model (CH). These values were chosen in order to have the iteration uncertainty always smaller than 0.1% for all variables in each simulation. Examples of convergence history are reported in fig.1-2 in terms of both residuals and total non-dimensional x-force (upper wall + bottom wall). The plots are drawn for both turbulence models.

Uncertainty assessment

The least squares root approach (Eca and Hoekstra, 2002, 2003) was used for uncertainty estimation for all the test cases computed. All the grids available in each grid set were considered to this end.

Test Case: Flow over a hill

The Reynolds number in the first test case is 60000, based on the hill height. The grids used range from 101×101 to 401×401. Grid shapes are shown in fig.3.

The solutions with SA and CH on both grid sets for the finest grid are reported in fig.4-7 in terms of pressure, axial velocity, eddy viscosity and streamlines. As it can be seen, the two solutions with the same turbulence model but different grid shape are very similar, the difference being of the same order of magnitude as the estimated uncertainty; nevertheless, there are remarkable differences between the predictions when changing the turbulence model. In particular, the recirculation bubble predicted with SA is much bigger than the one with CH.

The velocity profiles computed with SA and with all the grids in set A ranging from 101×101 to 401×401 are reported in fig.8

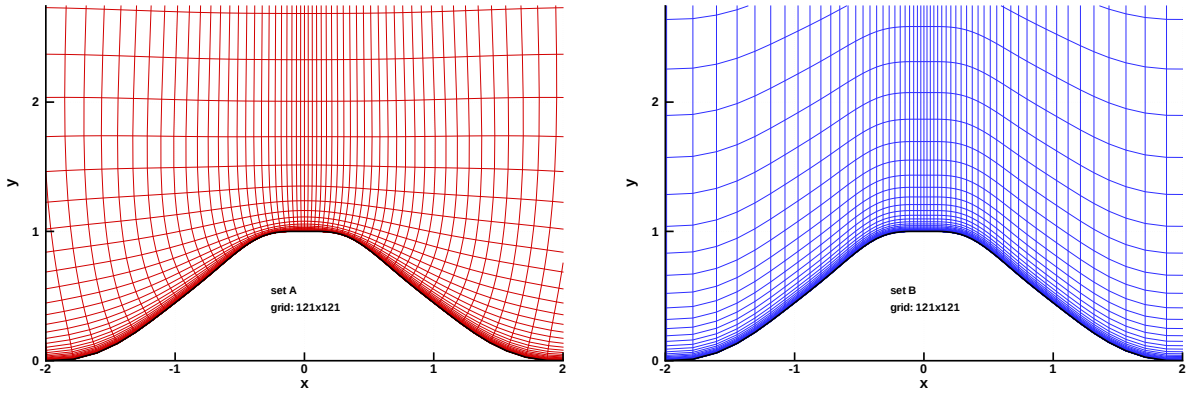

Figure 3: Hill: grid set A (left) and grid set B (right)

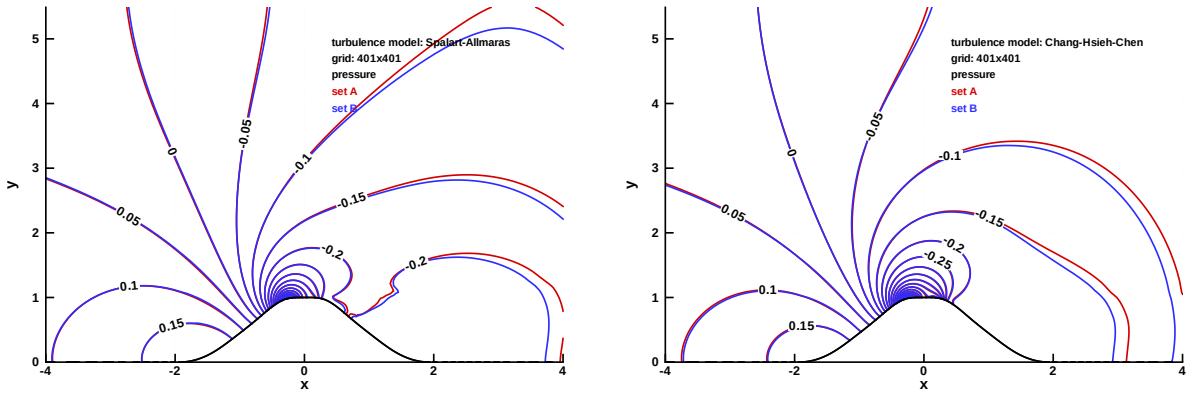

Figure 4: Hill - pressure contours: SA (left) and CH (right); Grid 401×401, set A (red) and B (blue)

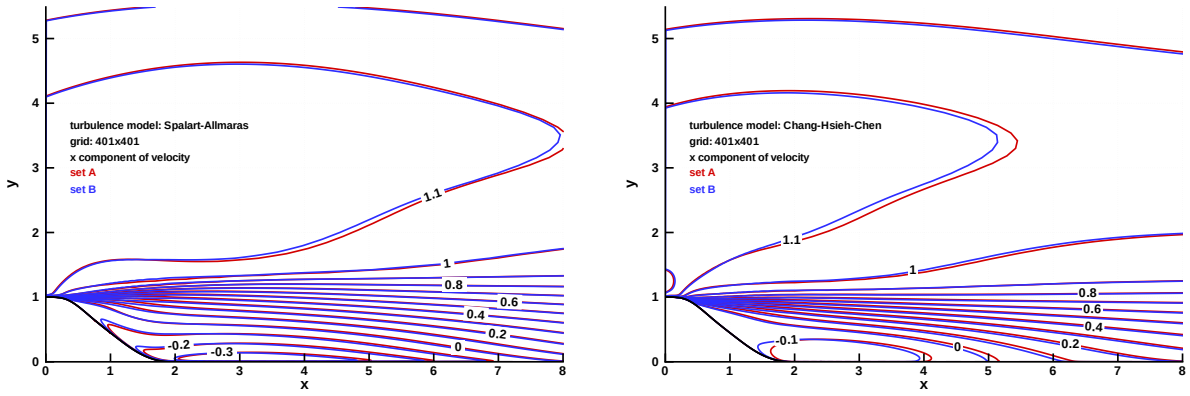

Figure 5: Hill - U contours: SA (left) and CH (right); Grid 401 × 401, set A (red) and B (blue)

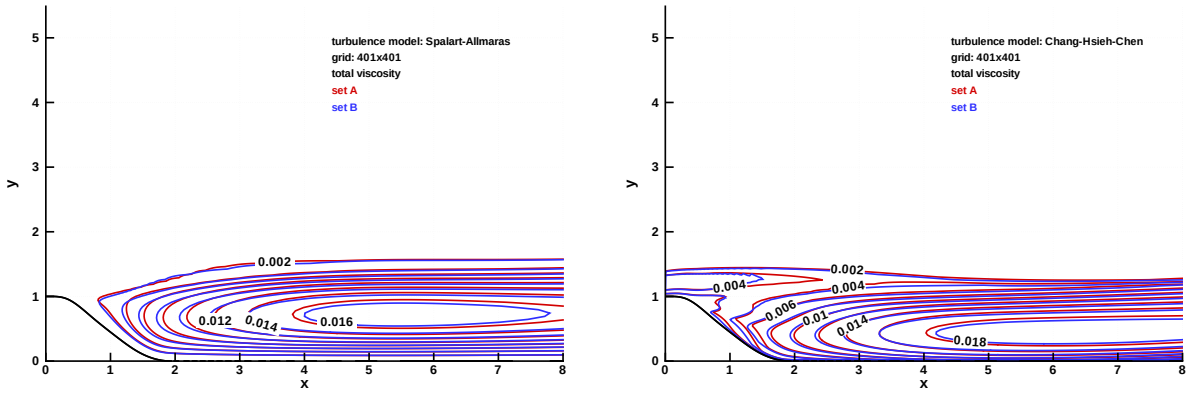

Figure 6: Hill - Eddy viscosity contours: SA (left) and CH (right); Grid 401 × 401, set A (red) and B (blue)

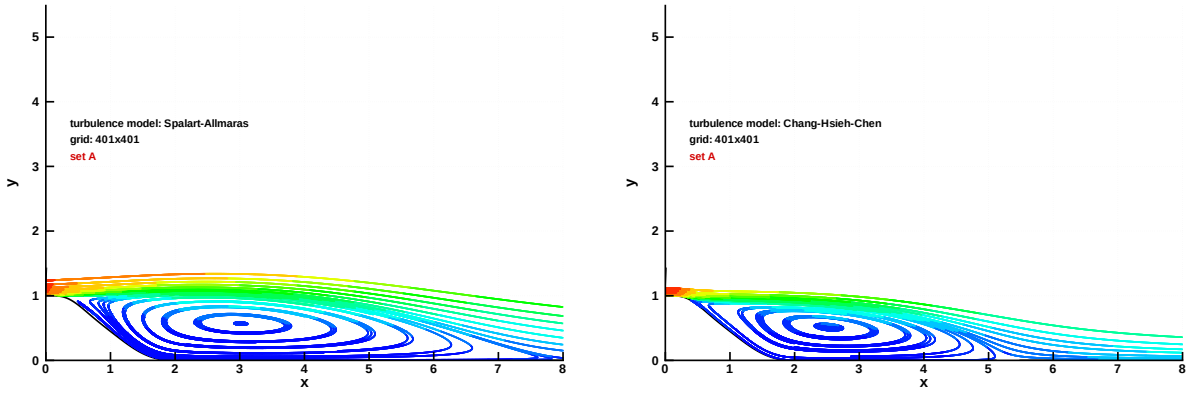

Figure 7: Hill - Streamlines: SA (left) and CH (right)

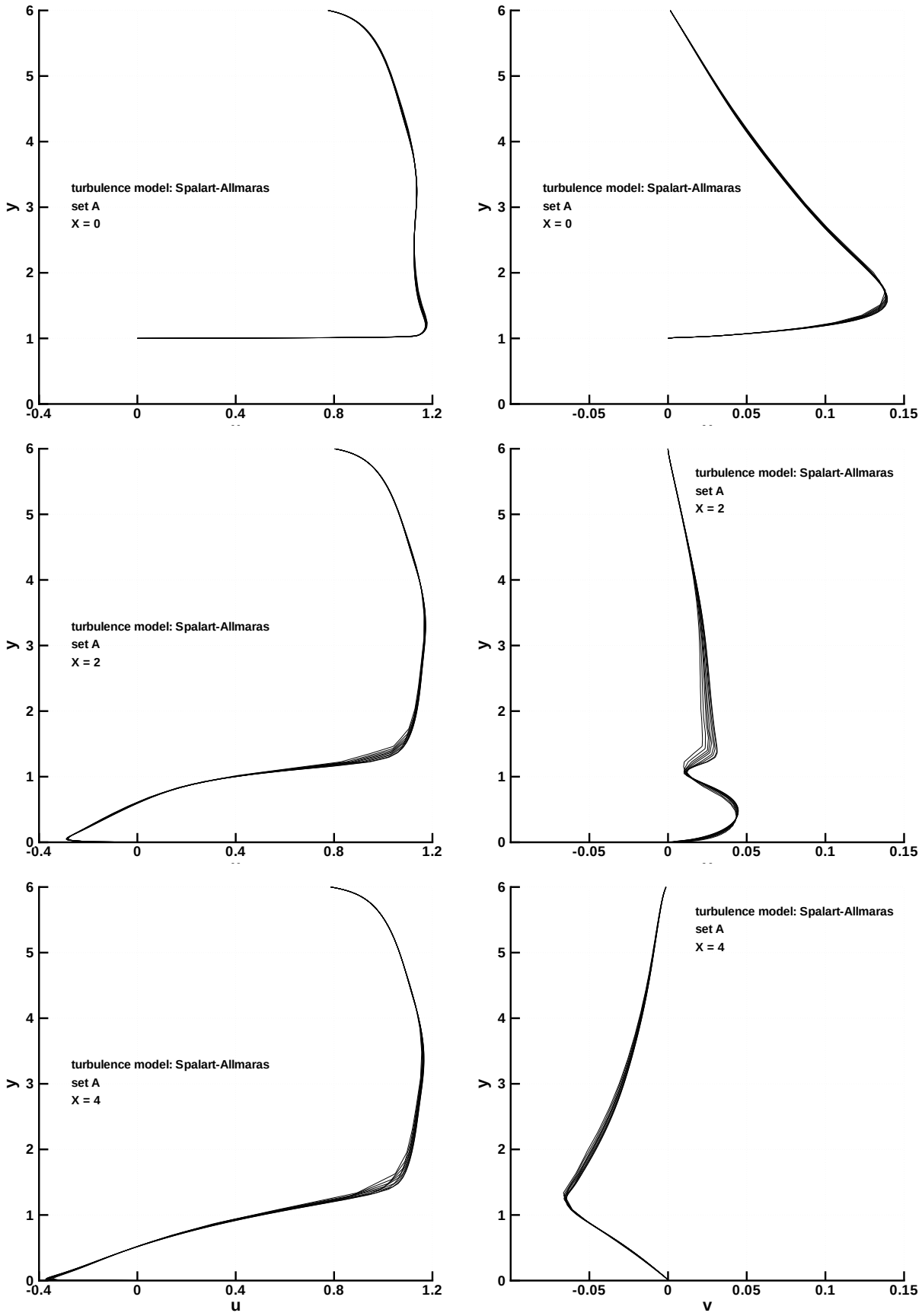

Figure 8: Hill - Velocity profiles computed with SA: u component (left) and v component (right) - Grid set A - Grid size : $101 \times 101, 121 \times 121, \ldots 361 \times 361, 401 \times 401$

The predicted values of friction and pressure resistance are reported in table 1 for the top wall and in table 2 for the bottom, whereas the location of separation and re–attachment points can be found in table 3. It can be seen that the values of resistance on the top are in good agreement which each other on all grids and with both turbulence models. On the bottom, instead, although the values predicted by each turbulence model overlap within the estimated uncertainty level on both grid sets, they differ significantly when comparing the solutions obtained with the two models. This is probably due to the different prediction of the separation bubble, as it can be deduced from table 3.

The uncertainty level was found to be of the same order of magnitude for both models and both grid sets; the same can be said about the observed converged order for the global quantities, which was estimated to range from 1.7 to 2.3 for both grid sets and models for resistance components, and from 1.4 to 1.9 for the location of the separation and re-attachment points.

R_f top	Predicted	Uncertainty	
SA - Set A	0.555×10^{-1}	0.50×10^{-3}	(0.9%)
SA - Set B	0.555×10^{-1}	0.34×10^{-3}	(0.6%)
CH - Set A	0.575×10^{-1}	0.86×10^{-3}	(1.5%)
CH - Set B	0.570×10^{-1}	0.46×10^{-3}	(0.8%)

Table 1: Hill: Friction resistance on the top wall. Results for SA and CH for all grid sets

R_f bottom	Predicted	Uncertainty		R_p bottom	Predicted	Uncertainty	
SA - Set A	0.232×10^{-1}	0.50×10^{-3}	(2.2%)	SA - Set A	0.194	0.20×10^{-3}	(0.1%)
SA - Set B	0.228×10^{-1}	0.84×10^{-3}	(3.7%)	SA - Set B	0.194	0.38×10^{-3}	(0.2%)
CH - Set A	0.580×10^{-1}	0.75×10^{-3}	(1.3%)	CH - Set A	0.163	0.52×10^{-2}	(3.2%)
CH - Set B	0.571×10^{-1}	0.40×10^{-3}	(0.7%)	CH - Set B	0.160	0.24×10^{-2}	(1.5%)

Table 2: Hill: Friction resistance and pressure resistance on the bottom wall. Results for SA and CH for all grid sets

X_{sep}	Predicted	Uncertainty		X_{reatt}	Predicted	Uncertainty	
SA - Set A	0.232×10^{-1}	0.50×10^{-3}	(2.2%)	SA - Set A	8.30	0.2	(2.4%)
SA - Set B	0.228×10^{-1}	0.84×10^{-3}	(3.7%)	SA - Set B	8.45	0.57	(7.0%)
CH - Set A	0.580×10^{-1}	0.75×10^{-3}	(1.3%)	CH - Set A	5.09	0.07	(1.4%)
CH - Set B	0.571×10^{-1}	0.40×10^{-3}	(0.7%)	CH - Set B	5.09	0.6	(12.%)

Table 3: Hill: Separation and re-attachment points. Results for SA and CH for all grid sets

Test Case: Flow over a backward facing step

The Reynolds number for this test case is 50000 based on the step height. The grids used range from 101×101 to 241×241. Grid shapes are shown in fig.9.

The computed solutions are reported in fig.10, 11, 12 and 13 in terms of pressure, eddy viscosity, streamlines and velocity profiles respectively. It can be observed that the dependence of the solution on the turbulence model is not as strong as in the previous test case, probably because the separation point here is determined by a geometrical factor rather than by boundary layer separation.

The predicted values of the friction and pressure resistance are summarized in table 4 for the top wall and in table 5 for the bottom, whereas the location of the re–attachment point is shown in table 6. Again, it can be seen that the values of resistance on the top are in reasonable agreement with each other on all grids and with both turbulence models, even if the difference between the predictions with the two models is higher than for the flow over the hill. The overlapping of data within the uncertainty level for the computations with the same model is observed also for this flow. As before, the friction resistance predicted with the $k - \varepsilon$ model is much larger than the one computed with the Spalart and Allmaras one-equation model. Also the prediction of the re–attachment point is rather different, the bubble computed with SA being about 15% longer than the one computed with CH.

As for the previous test case, the uncertainty level was found to be of the same order of magnitude for both models and the three grid sets; moreover, the uncertainty for the prediction of the pressure resistance was found to be rather high, in particular for the simulations using grid set C. The observed convergence order for the global quantities was found to be lower that for the flow over the hill, its values ranging from 0.7 to 1.7 for all quantities; in details, the lowest "actual" convergence order was observed for grid sets B and C, with values ranging from 0.7 to 1.2, whereas on grid set A it ranges from 1.0 to 1.7.

With regard to the local flow quantities, the uncertainty was rather large in percent values, although not too large if computed with respect to the reference quantities. In addition, grid convergence was not always observed, especially on grid sets B and C.

R_f top	Predicted	Uncertainty	
SA - set A	0.476×10^{-1}	0.75×10^{-3}	(1.6%)
SA - set B	0.495×10^{-1}	0.12×10^{-2}	(2.4%)
SA - set C	0.477×10^{-1}	0.11×10^{-2}	(2.3%)
CH - set A	0.550×10^{-1}	0.14×10^{-2}	(2.5%)
CH - set B	0.535×10^{-1}	0.14×10^{-2}	(2.6%)
CH - set C	0.546×10^{-1}	0.14×10^{-2}	(2.6%)

Table 4: Step: Friction resistance on the top wall. Results for SA and CH for all grid sets

R_f bottom	Predicted	Uncertainty		R_p bottom	Predicted	Uncertainty	
SA - set A	0.259×10^{-1}	0.31×10^{-3}	(1.2%)	SA - set A	0.107	0.97×10^{-2}	(9%)
SA - set B	0.269×10^{-1}	0.80×10^{-3}	(2.7%)	SA - set B	0.109	0.14×10^{-1}	(13%)
SA - set C	0.265×10^{-1}	0.45×10^{-3}	(1.7%)	SA - set C	0.099	0.17×10^{-1}	(17%)
CH - set A	0.515×10^{-1}	0.14×10^{-2}	(2.8%)	CH - set A	0.106	0.13×10^{-1}	(12%)
CH - set B	0.500×10^{-1}	0.15×10^{-2}	(3.0%)	CH - set B	0.108	0.15×10^{-1}	(14%)
CH - set C	0.515×10^{-1}	0.14×10^{-2}	(2.7%)	CH - set C	0.098	0.19×10^{-1}	(19%)

Table 5: Step: Friction resistance and pressure resistance on the bottom wall. Results for SA and CH for all grid sets

X_{reatt}	Predicted	Uncertainty		X_{reatt}	Predicted	Uncertainty	
SA - set A	6.04	0.20	(3.5%)	CH - set A	4.77	0.63	(13%)
SA - set B	5.80	0.21	(3.6%)	CH - set B	4.77	0.50	(11%)
SA - set C	5.92	0.23	(3.8%)	CH - set C	4.53	0.43	(9.5%)

Table 6: Step: re-attachment point. Results for SA and CH for all grid sets

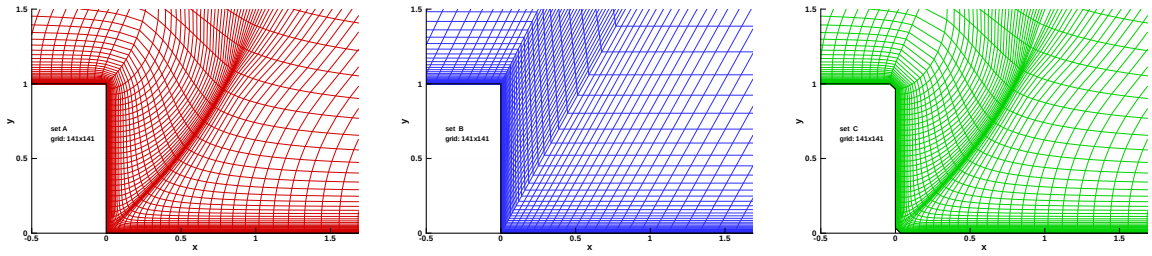

Figure 9: Step: grid set A (left), B (middle) and C (right)

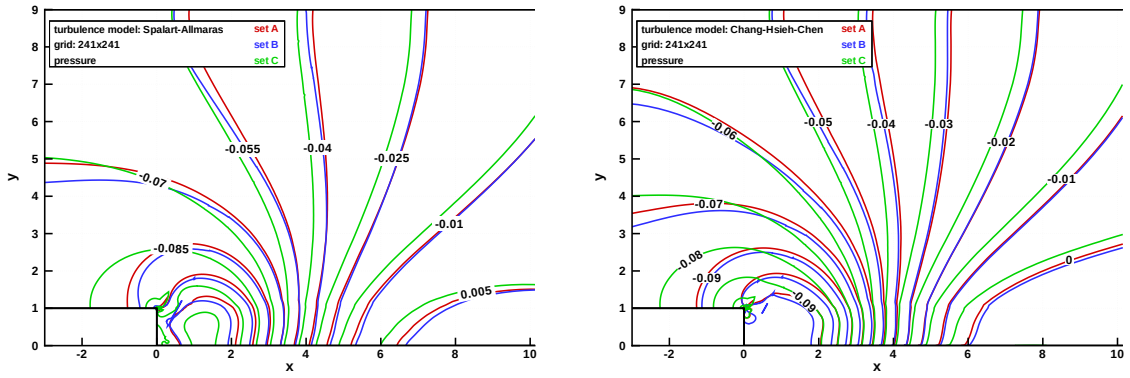

Figure 10: Step - pressure contours: SA (left) and CH (right) - set A (red), B (blue) and C (green)

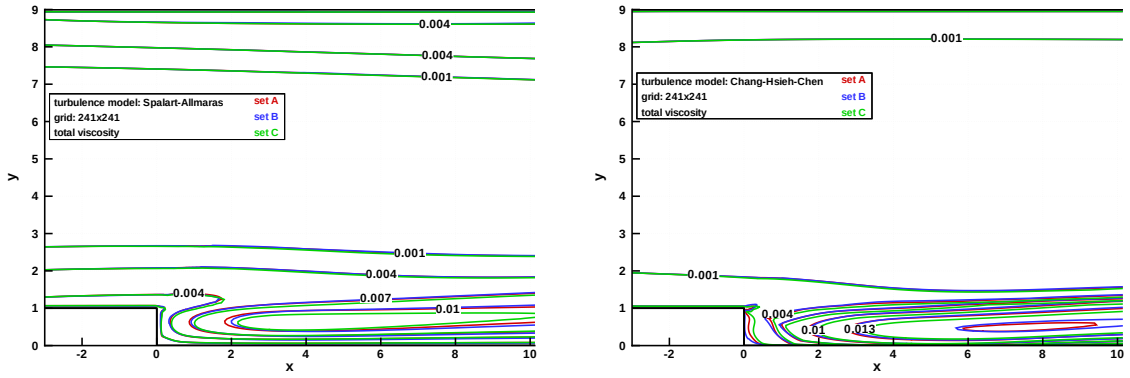

Figure 11: Step - Eddy viscosity contours: SA (left) and CH (right) - set A (red), B (blue) and C (green)

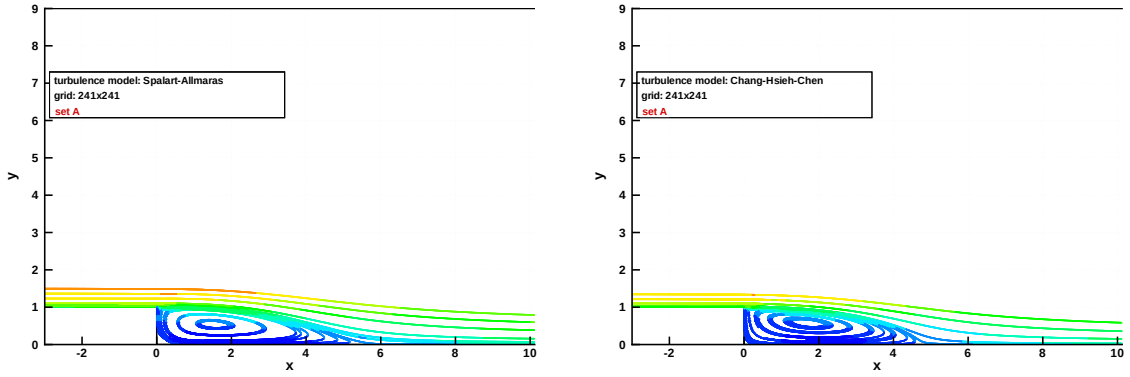

Figure 12: Step - Streamlines: SA (left) and CH (right)

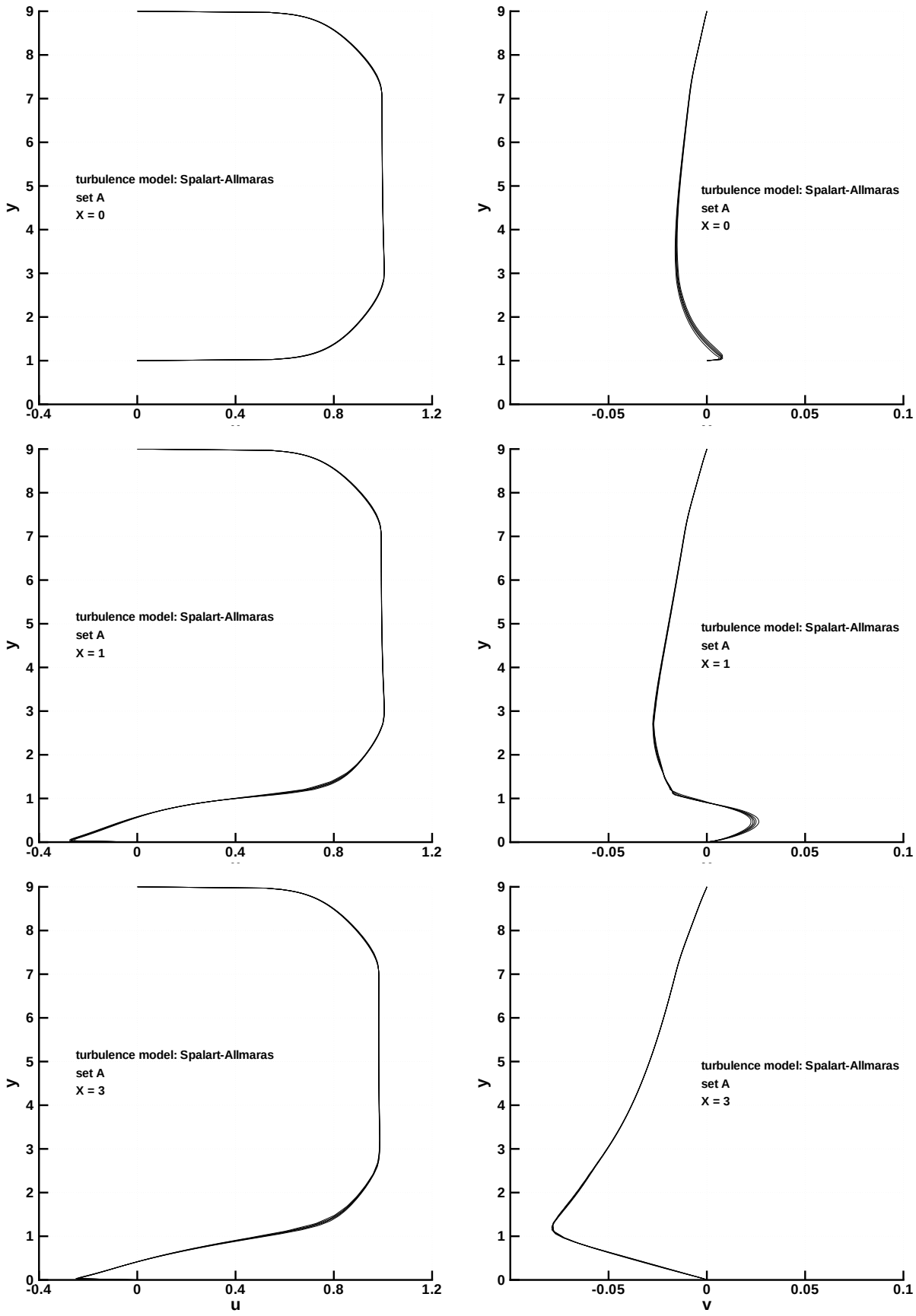

Figure 13: Step - Velocity profiles: u (left) and v (right) - Grid set A - Grid size $101 \times 101, 121 \times 121, \ldots 201 \times 201, 241 \times 241$

CONCLUSIONS

The numerical simulations of the flow over a hill (test case C-18 of the Ercoftac database) and past a backward facing step (test case C-30) were reported. The numerical scheme adopted is a second order E.N.O.-type scheme for the Eulerian part of the Navier-Stokes equation and a second order centered scheme for the viscous part. The discrete solution was computed by means of an implicit scheme with approximate factorization, coupled with local time step and a Full Multi Grid–Full Approximation Storage (FMG-FAS) approach.

The numerical simulation were performed with all the grids supplied for the Workshop and with two different turbulence models, namely the one-equation model by Spalart and Allmaras (1994) and the two-equation $k - \varepsilon$ model by Chang et al. (1995).

The approach used for the assessment of the numerical uncertainty is the one described in Eca and Hoekstra (2002, 2003), based on a least squares root procedure.

It was observed that the solutions significantly depend on the turbulence model, whereas they overlap within the uncertainty range with respect to grid size and shape.

The numerical uncertainty was comparable for all grid shapes and models, the highest values having been observed in the prediction of the pressure resistance and for local quantities for the flow over a backward facing step. Grid convergence was not always obtained for the prediction of some local quantities in the second test case, especially for grid set B and C.

References

Beam, R. and Warming, R. (1978). An Implicit Factored Scheme for the Compressible Navier-Stokes Equations. *AIAA Journal*, 16:393–402.

Brandt, A. (1984). *Multi-grid Techniques: 1984 Guide with Application to Fluid Dynamics*. The Weizmann Institute of Science, Rehovot (Israel).

Chang, K. C., Hsieh, W. D., and Chen, C. S. (1995). A Modified Low–Reynolds–Number Turbulence Model Applicable to Recirculating Flow in Pipe Expansion. *J. Fluid Eng.*, 117:417–423.

Chorin, A. (1967). A Numerical Method for Solving Incompressible Viscous Flow Problems. *J. Comput. Phys.*, 2:12–26.

Di Mascio, A., Broglia, R., and Favini, B. (2001). *A Second Order Godunov–Type Scheme for Naval Hydrodynamics*, pages 253–261. Kluwer Academic/Plenum Publishers.

Eca, L. and Hoekstra, M. (2002). An Evaluation of Verification Procedures for CFD Applications. In *Proc. of the* 24^{th} *Symposium of Naval Hydrodynamic*, Fukuoka, Japan.

Eca, L. and Hoekstra, M. (2003). Uncertainty Estimation: A Grand Challenge for Numerical Ship Hydrodynamics. In *Proc. of the* 6^{th} *Numerical Towing Tank Symposium*, Rome, Italy.

Favini, B., Broglia, R., and Di Mascio, A. (1996). Multi–grid Acceleration of Second Order ENO Schemes from Low Subsonic to High Supersonic Flows. *Int. J. Num. Meth. Fluids*, 23:589–606.

Godunov, S. (1959). A Finite Difference Method for the Numerical Computation of Discontinuous Solutions of the Equations of Fluid Dynamics. *Mat. Sb.*, 47:271.

Harten, A., Engquist, B., Osher, S., and Chakravarthy, S. R. (1987). Uniformly High Order Accurate Essentially Non–Oscillatory Schemes. *J. Comput. Phys.*, 71:231–303.

Spalart, P. R. and Allmaras, S. R. (1994). A One–Equation Turbulence Model for Aerodynamic Flows. *La Recherche Aérospatiale*, 1:5–21.